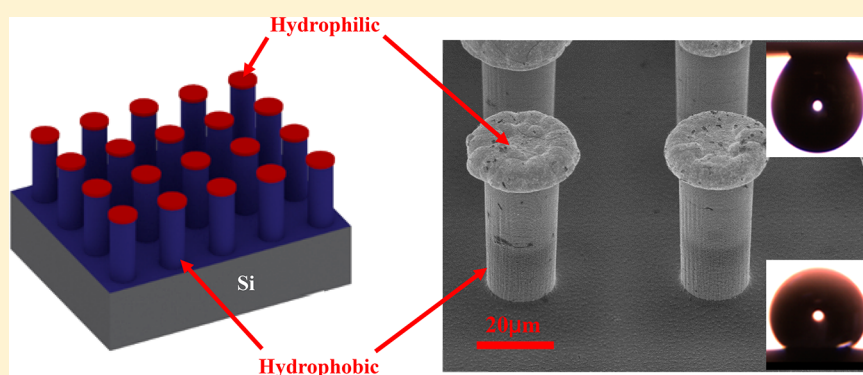# Salvinia-Effect-Inspired "Sticky" Superhydrophobic Surfaces by Meniscus-Confined Electrodeposition

Deyin Zheng,[†] Youhua Jiang,[‡] Wentao Yu,[†] Xiufen Jiang,[†] Xin Zhao,[†] Chang-Hwan Choi,[‡] and Guangyi Sun*,[†]

[†]Institute of Robotics and Automatic Information System &Tianjin Key Laboratory of Intelligent Robotics, Nankai University, Tianjin 300071, People's Republic of China

[‡]Department of Mechanical Engineering, Stevens Institute of Technology, Hoboken, New Jersey 07030, United States

S *Supporting Information*

ABSTRACT: Inspired by the Salvinia effect, we report the fabrication and characterization of a novel "sticky" superhydrophobic surface sustaining a Cassie−Baxter wetting state for water droplets with high contact angles but strong solid−liquid retention. Unlike superhydrophobic surfaces mimicking the lotus or petal effect, whose hydrophobicity and droplet retention are typically regulated by hierarchical micro- and nanostructures made of a homogeneous material with the same surface energy, our superhydrophobic surface merely requires singular microstructures covered with a hydrophobic coating but creatively coupled with hydrophilic tips with different surface energy. Hydrophilic tips are selectively formed by meniscus-confined electrodeposition of a metal (e.g., nickel) layer on top of hydrophobic microstructures. During the electrodeposition process, the superhydrophobic surface retains its plastron so that the electrolyte cannot penetrate into the cavity of hydrophobic microstructures, consequently making the electrochemical reaction between solid and electrolyte occur only on the tip. In contrast to typical superhydrophobic surfaces where droplets are highly mobile, the "sticky" superhydrophobic surface allows a water droplet to have strong local pinning and solid−liquid retention on the hydrophilic tips, which is of great significance in many droplet behaviors such as evaporation.

■ INTRODUCTION

Superhydrophobic surfaces have attracted tremendous attention for the past couple of decades due to their unique properties, such as water-repellent,[1−3] self-cleaning,[4−7] antifouling,[8,9] anticorrosion,[10−12] anti-icing,[13−16] and enhanced heat and mass transfer[17−21] properties. More recently, it has also been experimentally proven that a well-designed superhydrophobic surface can produce significant drag reduction in liquid flows.[22−24] Such unique properties result from the air layer entrained between the hydrophobic structures on the surface. Thus, the stability and longevity of the entrapped air layer are important for such applications.[25] Although various superhydrophobic surfaces have been proposed and fabricated using different methods,[26−29] the surfaces can generally be classified into slippery or sticky superhydrophobic surfaces based on the dynamic mobility of a droplet on the surfaces[26,30] compared to that on a flat surface. They are also commonly referred to as the lotus or petal effect,[27,31−33] respectively, according to the significance of contact angle hysteresis or droplet retention.[34−36] In such surface systems, hierarchical or dual-scale (e.g., micrometer and nanometer) structures play an important role in determining the different wetting and adhesion properties.[33,37] On the other hand, the wetting and adhesion behaviors are dependent not only on the geometric structures of the surface but also on the chemical composition of the surface, i.e., surface energy.[33,35] To date, most researches on artificial superhydrophobic surfaces with high droplet retention have focused on the geometrical influences. As a result, it has been widely accepted that the coexistence of high contact angle and high contact angle hysteresis must be

obtained by mimicking the rose-petal-like hierarchical structures, where the cavity of microstructures must be wetted while the nanostructures hierarchically added on the microstructures remain nonwetted.[38,39] Notably, most rose-petal-like artificial superhydrophobic surfaces are either made of or coated with a homogeneous hydrophobic material, which has almost become a technical standard in the field. However, if one looks back to the old question of what the origin of contact angle hysteresis should be, one would realize that a simple truth has long been neglected, which is that contact angle hysteresis originates from hydrophilic chemical defects[35,36,40] and the inhomogeneity of surface energy.

Recently, in the field of biology, a few reports have shown that for some plants and vegetables, e.g., Salvinia and allium, their leaves support droplets with high contact angle as well as high contact angle hysteresis,[33] which is not because of the geometrical factor but because of the presence of "adhesive" pins with different surface energy. Such a heterogeneous superhydrophobic surface with hydrophilic pins can provide unique wetting properties and applicability, even superior to the typical superhydrophobic surfaces with homogeneous surface energy. For example, it has been demonstrated that hydrophilic pins of fern Salvinia can help stabilize the air layer by pinning the air−water interface underwater, preventing the loss of air from the surface especially in a turbulent flow condition.[22,33] This provides an intriguing perspective for developing a long-term air-retaining superhydrophobic surface, which is especially crucial for underwater applications. Moreover, the heterogeneous superhydrophobic surfaces with hydrophilic pins are of high scientific interest for enhanced heat transfer.[17] Despite the promising properties, the fabrication of artificial superhydrophobic surfaces with hydrophilic pins has been rarely reported, mainly due to the difficulties of making such inhomogeneous surface structures with regulated surface energy on a micrometer or nanometer scale.[41−43]

In this work, we propose a feasible method to fabricate such a heterogeneous superhydrophobic surface textured with microstructures that are selectively decorated with hydrophilic tips. We investigate a novel meniscus-confined electrodeposition process to grow a thin layer of hydrophilic metal only on the top of the hydrophobic microstructures, while keeping the rest part of the microstructures intact. The key innovative idea is to utilize the meniscus-confined liquid−solid contact on the superhydrophobic surface to selectively localize the electrochemical reaction during electrodeposition process. Even fully immersed in the electrolyte, the superhydrophobic surface retains its plastron, and the electrolyte cannot penetrate into the cavity of microstructures. Consequently, the electrochemical reaction between solid structure and electrolyte occurs only on the tip. This method requires only one additional fabrication step of a regular electrodeposition process to form hydrophilic tips for an existing superhydrophobic surface. Whereas a localized electrodeposition process based on a meniscus shape had previously been reported,[44−46] in those studies the guidance of electrodeposition relied mostly on the usage of a single free-standing micrometer scale metal (e.g., platinum) wire integrated with precisely controlled X-Y-Z stages and an electrolyte dispensing system, making them not feasible for the fabrication of large-area dense arrays. Here, we use the similar principle of the meniscus-confined solid−liquid interface which is the inherent property of a pre-existing superhydrophobic surface. However, the novelty of our scheme is not to use such additional systems as the nozzle of

micropipet but to realize the meniscus-confined solid−liquid interface using the autonomous gas-retaining mechanism of an immersed superhydrophobic surface itself. To demonstrate the feasibility of the newly developed heterogeneous superhydrophobic surface with hydrophilic tips and characterize its uniqueness compared to typical (e.g., homogeneous) superhydrophobic surfaces, underwater wetting property, apparent contact angles, and the retention of laterally sliding and evaporating droplets on such surfaces are investigated.

■ FABRICATION SCHEME

Figure 1 shows the overall fabrication scheme of the proposed heterogeneous superhydrophobic surface. First, micropost
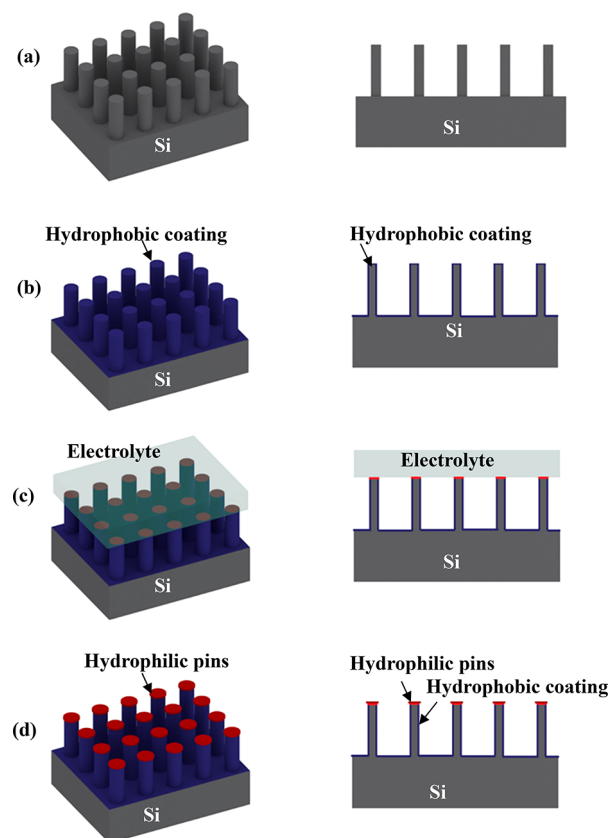

Figure 1. Fabrication process of a heterogeneous superhydrophobic surface with hydrophilic tips, drawn schematically but not to scale. (a) Fabrication of micropost structures of silicon using conventional photolithography and deep reactive ion etching (DRIE). (b) Hydrophobic coating on microstructures. (c) Meniscus-confined electrodeposition. (d) Final superhydrophobic surfaces with hydrophilic tips.

patterns of silicon are formed by using conventional photolithography and deep reactive ion etching (DRIE) processes (Figure 1a). In order to make the surface hydrophobic and retain air layer between the microstructures to support the Cassie−Baxter superhydrophobic state, Teflon solution (0.05 wt % Teflon AF1600 in FC 40) is applied on the DRIE-etched silicon surface (Figure 1b). During the electrodeposition process (Figure 1c), the superhydrophobic surface retains its gas plastron so that the electrolyte makes the contact with only the top surface of the microposts. The electrolyte cannot penetrate into the cavity of microstructures due to the entrained gas plastron and consequently make the electro-

chemical reaction between solid and electrolyte occur only on the tips. Figure 1d shows the schematic of the processed sample.

■ EXPERIMENTAL SECTION

Fabrication of Micropost Structures. As for the silicon substrate, silicon wafer with a relatively low resistivity was employed to allow a wide-range plating current in the electrodeposition step. Single-side-polished, 4 in., 500 ± 5 μm thick $\langle 100 \rangle$ silicon wafers of p-type with resistivity less than 0.01 ohm·cm were used as the substrates. First, the wafer was cleaned using a standard piranha (mixture of H_2SO_4 and H_2O_2, 4:1 in volume) and buffered oxide etch (BOE) solutions to remove the organic residue and native oxide layer, respectively. After the cleaning, hexamethyldisilazane (HMDS) was coated on the surface using a vapor deposition method to serve as an adhesion promote layer for photoresist polymer. Then, 1.5 μm thick protective layer of photoresist (A Z5214, Microchemicals) was spin-coated on the wafer (4000 rpm for 30 s). The wafer was then soft-baked on a hot plate at 95 °C for 90 s. To pattern microstructure arrays on the photoresist layer, the photoresist layer was exposed to ultraviolet (UV) light through a photomask by using a mask aligner (MA6, Karl Suss, Germany) in a proximity contact mode and then developed by immersing the wafer in the developer (RZX-3038, SUZHOU RUIHONG CO., Ltd.). The developed wafer was then hard-baked on a hot plate at 110 °C for 2 min. The micropost structures were formed by a DRIE process using an inductively coupled plasma etching machine (Surface Technologies Systems USA Inc., Redwood, CA). The detailed recipe of the DRIE process is shown in Table S1 of the Supporting Information. After the DRIE step, the photoresist and polymer residues were removed by piranha, and the native oxide layer on the silicon wafer was further cleaned by BOE.

Hydrophobic Coating. Teflon was used for the hydrophobic coating of the microstructured surface. Teflon AF 1600 was purchased from Dupon Company. Teflon AF 1600 can be dissolved in perfluorinated solvents for the coating of highly uniform and thin films. In this study, Teflon solution (0.05 wt %) was prepared by mixing the AF1600 powders in FC-40 solution (Sigma-Aldrich). The mixture was stirred with a magnetic stirrer for 12 h to completely dissolve the Teflon power to the perfluorinated solvent. Teflon solution (3 μL) was applied the microstructured silicon substrate (1 × 1 cm^2) using a micropipet, giving the Teflon coating thickness of ~5 nm. Then the substrate was baked on a hot plate at 170 °C for 10 min, followed by another baking step at 330 °C for 1 h.

Meniscus-Confined Electrodeposition. The schematic illustration of the meniscus-confined electrodeposition process is shown in Figure 2. The micropatternerd superhydrophobic silicon substrate was cut into small rectangular chips of 1.5 × 1.5 cm^2, where the effective area of the microstructures is 1 × 1 cm^2. Then, the edge and backside of the chip were covered with a protective tape (1712#, 3M, USA) to prevent the electrodeposition in those areas. Electroplating solution
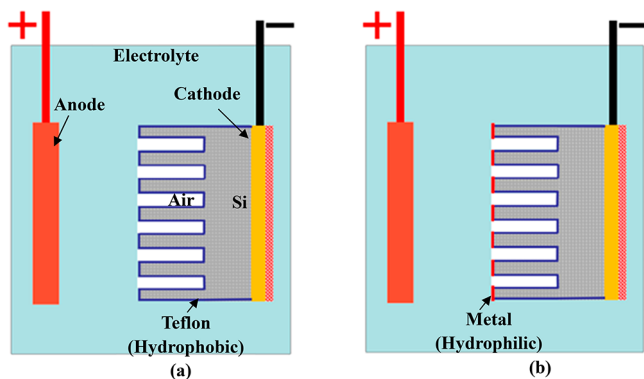
(Watts Nickel, 25% NiSO$_4$; 5% NiCl$_2$; 5% H$_3$BO$_3$; 65% H$_2$O) was purchased from TRANSENE Company (Denvers, MA). A Keithley Model 2425 sourcemeter was used as the current source. During the electrodeposition, a nickel sheet with the same footprint size to the chip was used as anode and placed in parallel with the silicon chip (cathode) to ensure a uniform current density on the surface. The applied bias current between the anode and cathode is a key factor of the electrodeposition process. Because of the dielectric property of the Teflon, the Teflon film works as an insulating layer between the electrolyte and silicon substrate. The dielectric constant of Teflon AF is the lowest of any known solid polymers, ranging from 1.89 to 1.93, and the breakdown voltage is ~20 V/μm for AF 1600 at 23 °C.[47] At the start of the electrodeposition, the bias current value was set at a relatively high level of 120 mA (i.e., 120 mA/cm^2 as a current density over the 1 × 1 cm^2 surface area) to break down the Teflon layer on the structural tops and applied until the actual current value reached the set value (120 mA). Considering the coating thickness of Teflon (~5 nm) and the breakdown voltage (~20 V/μm), the Teflon AF 1600 layer is easy to break down by the actuating voltage. There is effectively no electric current to the sidewalls due to the entrapped air. Thus, the breakdown of the Teflon layer should be occurred only at the silicon–electrolyte interface. In general, it takes less than 5 s for the current value to reach the set value from zero, and the final values of current and voltage at this phase are 120 mA and 8.3 V. According to the Faraday's laws of electrolysis, the amount of mass changes produced by the bias current is proportional to the quantity of the electricity that passes. Therefore, the mass of the deposited nickel depends on the duration of electrodeposition and the current value. Then the current was set at a lower level of ~20 mA (i.e., 20 mA/cm^2 over the surface area) and applied for 5 min to ensure the uniform density and smoothness of the electroplated metal layer. After the electrodeposition process, the sample was rinsed with deionized water and then dried by nitrogen gas.

Measurement of Surface Morphology and Chemical Composition. The morphology of fabricated microstructures of the surfaces was analyzed by using a field-emission scanning electron microscope (S-4800 FE-SEM, Hitachi). The chemical composition of the microstructures was analyzed by using the energy dispersive spectrometer (EDS, JSM-7500F, JEOL).

Underwater Immersion Test. The underwater test was carried out by immersing the microstructured samples in water. First, the samples were partially immersed in water for the visualization of the light reflection of the air cushion entrained on the samples' surfaces. The images were taken at ~45° to the surface of the samples. Then the samples were fully immersed in water (~3 cm deep), and air bubbles were continuously blown to the samples' surfaces by a dropper to examine the stability of the air cushion and the wetting transition.

Measurement of Contact Angles. Contact angles were measured by using an in-house contact angle meter with image processing software (Digimizer) at room condition (air temperature, 25 °C; air humidity, 54%; air pressure, 100 kPa). A deionized water droplet of 4 μL was taken into contact with the surfaces to measure contact angles. Two different kinds of surfaces were prepared and tested for comparison: one is the superhydrophobic surface without the decoration of hydrophilic tips, and the other is the super-hydrophobic surface decorated with hydrophilic tips. The contact angles were measured at ten different locations over the surface of the given same sample to get their average and standard deviation values. The contact angle hysteresis was measured using a droplet dragging method.[48] The surfaces were mounted on a moving stage, while the needle was fixed within the view of the CCD camera. As the stage moved, the droplets were dragged by the needle. During the stage moving, the advancing and receding angles of the droplets were measured to estimate the contact angle hysteresis. The sliding angles were measured by mounting the surfaces on a tilting stage. The sliding angles were obtained by tilting the stage until the droplet just began to move. The droplet volume used to measure sliding angles was ~4 μL.

Droplet Evaporation Test. To see the effects of the hydrophilic tips of the heterogeneous superhydrophobic surface compared to the homogeneous superhydrophobic surface with no decoration with the
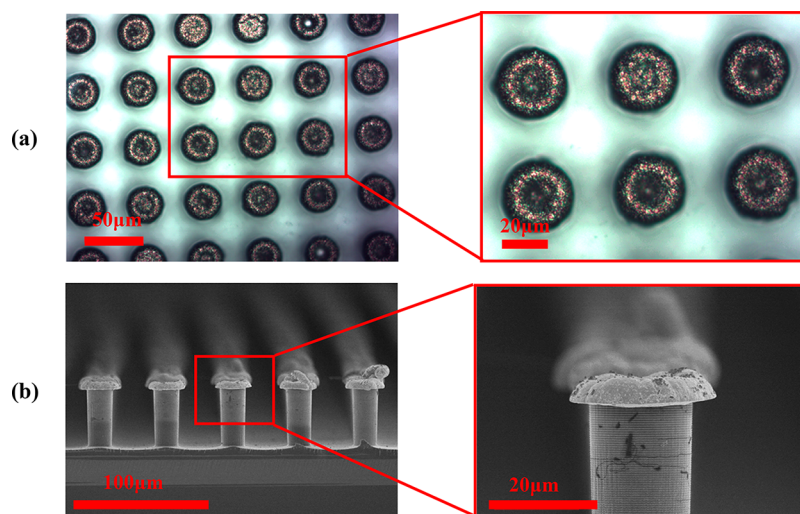

Figure 2. Schematic illustration of meniscus-confined electrodeposition: (a) before electrodeposition; (b) after electrodeposition.

Figure 3. Morphology of the hydrophilic metal (nickel) tips fabricated on the hydrophobic micropost structures. (a) Optical images (top views) of the microposts. (b) Scanning electron microscope (SEM) images (side views) of the microposts.

hydrophilic tips, the droplet evaporation tests were also performed on the surfaces. During the evaporation, the evaporation kinetics was measured by analyzing the changes of droplet profile, volume, contact angles, and contact diameters. At the start of the experiments, 4 μL of deionized water droplets were placed on the surfaces. Then, the droplet profiles were recorded with a CCD camera by taking images every 2 min to measure the droplet volumes, contact angles, and contact diameters, until the droplets were dried out. All the experiments were performed under the same room condition (air temperature, 25 °C; air humidity, 54%; air pressure, 100 kPa).

RESULTS AND DISCUSSION

Microstructures Fabricated by the Meniscus-Confined Electrodeposition. Figure 3 shows the optical and SEM images of the heterogeneous superhydrophobic surfaces with hydrophilic tips of nickel fabricated by the meniscus-confined electrodeposition process. Figure 3 shows that nickel tips are formed on the tips of the microposts. The electrodeposited nickel is thicker around the edge than in the center and has a flat bottom in the overhang part, indicating the proposed meniscus-confined electrodeposition method successfully form the nickel tips on the top of the microposts. In the Cassie−Baxter superhydrophobic wetting state, the geometry of the electrolyte meniscus is not a regular 2D plane so that the current does not distribute uniformly over the interface. In the beginning of the electrodeposition, the current is inclined to concentrate at the sharp edges and pass more readily through these regions than the others,[49] so that the deposition generally starts from the sharp edges (see Figure S1 in the Supporting Information). Thus, the nickel gets deposited over the top surface in an anisotropic way, and the thickness of the nickel layer is non-uniform over the surface. As shown in Figure 3b (see also Figure S2), the electrodeposited nickel is thicker around the edge than in the center and has a flat bottom in the overhang part.

For the selective local deposition of the hydrophilic nickel tips on the structural tops, the Cassie−Baxter wetting state is crucial to the process. In the Cassie−Baxter wetting state, the electrolyte only contacts with the upper part of the micropost structures of the superhydrophobic surface with trapped air cushion underneath. The localized silicon−electrolyte interface ensures that the nickel layer deposits only on the upper part of the microposts. The hydrophobic coating of Teflon supports

and sustains the Cassie−Baxter wetting state for the electrolyte solution during the electroplating process. The electrolyte solution is water-based aqueous solution, and the contact angles of the electrolyte droplets on the Teflon-coated micropost surfaces were almost similar to those of water droplets (see Figure S3), indicating the Cassie−Baxter superhydrophobic wetting state should be maintained with the electrolyte. It was also confirmed by the light reflection from the surface when the samples were immersed in the electrolyte solution. Even when the Teflon-coated microstructured substrate was fully immersed in the electrolyte, the air cushion was visible due to the mirror-like light reflection at the liquid−air interface, verifying the Cassie−Baxter wetting state.[50−52] If the electrolyte penetrates into the cavities of the microstructure, the light reflection decreases. Once the cavities are fully filled with the electrolyte (i.e., Wenzel state), the original color of the substrate is visible. In the Wenzel state, the liquid−air meniscus no longer exists, and the electrolyte contacts with the entire surface of the micropost structures. For comparison, the electrodepositing process was also applied in the Wenzel state, which was achieved by adding surfactant (Photo-Flo 200, Kodak) to the electrolyte solution. As shown in Figure S4, nickel get deposited onto sidewalls as well as the top surfaces, which indicates the collapse of the Cassie−Baxter wetting state.

As a further verification to the localized electrodeposition, qualitative elemental analysis was performed using an energy dispersive spectroscopy (EDS) technique. Figure 4 shows the SEM and EDS mapping images of the heterogeneous superhydrophobic surface selectively decorated with the nickel hydrophilic tips. Figures 4b and 4d show that the nickel only exists on the tips of the microposts, demonstrating that the proposed meniscus-confined method is an effective way to localize the electrodeposition process. Moreover, Figure 4e shows that fluorine (F) is distributed only on the sidewalls and bottoms of the microstructure, indicating the presence of the Teflon coating. It also suggests that the Teflon coating keeps good adhesion to the surfaces, which do not have any direct contact with the electrolyte or rinsing water during the fabrication processes due to the entrained air layer supported by the Cassie−Baxter superhydrophobic wetting state.

Underwater Wetting Properties. An underwater immersion test was performed to investigate the effect of the
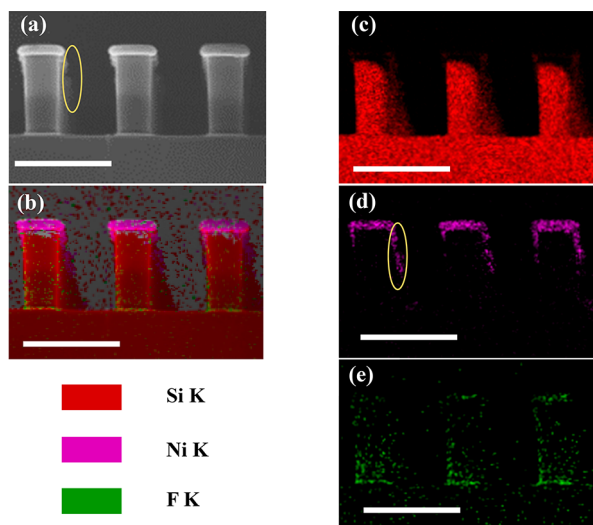
Figure 4. EDS images of the superhydrophobic surface with hydrophilic tips. (a) SEM image, where the ellipse indicates the nickel tips of the post array behind the post in the front. (b) Layered image of element distribution. (c) Distribution of Si. (d) Distribution of nickel, where element distribution inside the ellipse comes from the posts behind. (e) Distribution of fluorine (F). All the images are in the same field of view. Scale bar in each image is 50 μm.

hydrophilic tips on the underwater wetting properties. Figure 5 shows the images of the superhydrophobic surfaces without and
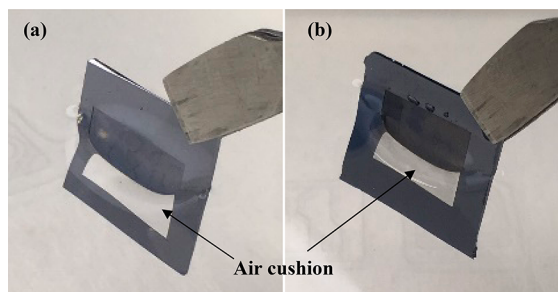

Figure 5. Underwater immersion test. (a) Superhydrophobic surface without the decoration of hydrophilic tips. (b) Superhydrophobic surface decorated with hydrophilic tips.

with hydrophilic tips partially immersed in water. The bright reflection of the underwater part of the surfaces indicates the total internal reflection of light that results from the gas layer retained on the superhydrophobic surfaces. The results show that there is no significant change in the appearance of the light reflection between the homogeneous superhydrophobic surface and the heterogeneous superhydrophobic surface selectively decorated with hydrophilic tips, suggesting that the Cassie–Baxter wetting state is also well maintained on the heterogeneous superhydrophobic surfaces decorated with the hydrophilic tips. It also indirectly indicates that the hydrophilic metal tips are present only on the tips of microposts. The sidewalls and the bottom of the microposts are still hydrophobic with the presence of Teflon coating, making these areas unwetted by water and support the Cassie–Baxter wetting state. This is a significant difference from the conventional "sticky" or Wenzel-state superhydrophobic surfaces. Similar to the case of electrolyte, for a superhydrophobic surface in the Cassie–Baxter state, the trapped air on the surface is visible due

to the total internal reflection of light at the water–air interface. When the suspended liquid–gas interface collapses, the wetting state transits from the Cassie–Baxter state to the Wenzel state, in which the internal reflection of light disappears and no mirror-like reflection is observed. To evaluate the underwater stability of the air cushion, we also compared the surfaces without and with hydrophilic tips by blowing air bubbles to the surfaces under full immersion. The Cassie–Baxter state is easy to collapse with flow disturbance and shows wetting transition on the homogeneous superhydrophobic surface (see Movie 1 in the Supporting Information), while the Cassie–Baxter state shows better stability on the heterogeneous superhydrophobic surface with the hydrophilic tops (see Movie 2). The results agree with the previous report that the hydrophilic pins of could help stabilize the air layer by pinning the air–water interface underwater.[33]

Contact Angles and Droplet Mobilities. Figure 6 shows the profiles of water droplets on the superhydrophobic surfaces
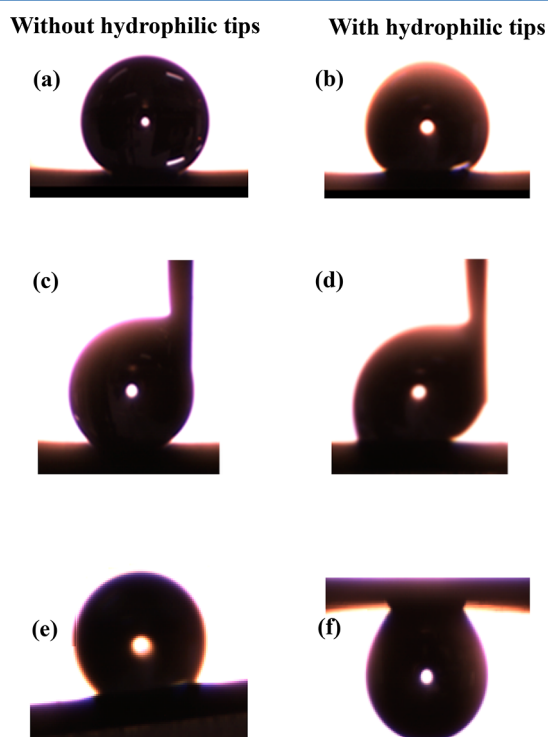

Figure 6. Profiles of water droplets on (a, c, e) the superhydrophobic surface with no decoration of hydrophilic tips and (b, d, f) the superhydrophobic surface with decoration of hydrophilic tips. (a, b) Measurement of apparent static contact angles. (c, d) Measurement of apparent advancing and receding contact angles by dragging water droplets on the surfaces. (e, f) Tilting test for the measurement of sliding angles.

without and with hydrophilic tips, measured for the apparent contact angles and sliding angles. The measured values are also summarized in Table 1. The static contact angles (Figure 6a,b) were measured as soon as the droplets were placed on the surfaces using a needle, and they were $146 \pm 2°$ and $148 \pm 2°$ on the surfaces without and with hydrophilic tips, respectively. Even with the hydrophilic tips, no significant difference was observed in the static contact angles. However, the surfaces show different properties in the measurements of advancing/receding contact angles in the dragging experiment (Figure 6c,d). The advancing and receding contact angles measured on

Table 1. Comparison of Wetting Properties of the Superhydrophobic Surfaces without and with Hydrophilic Tips

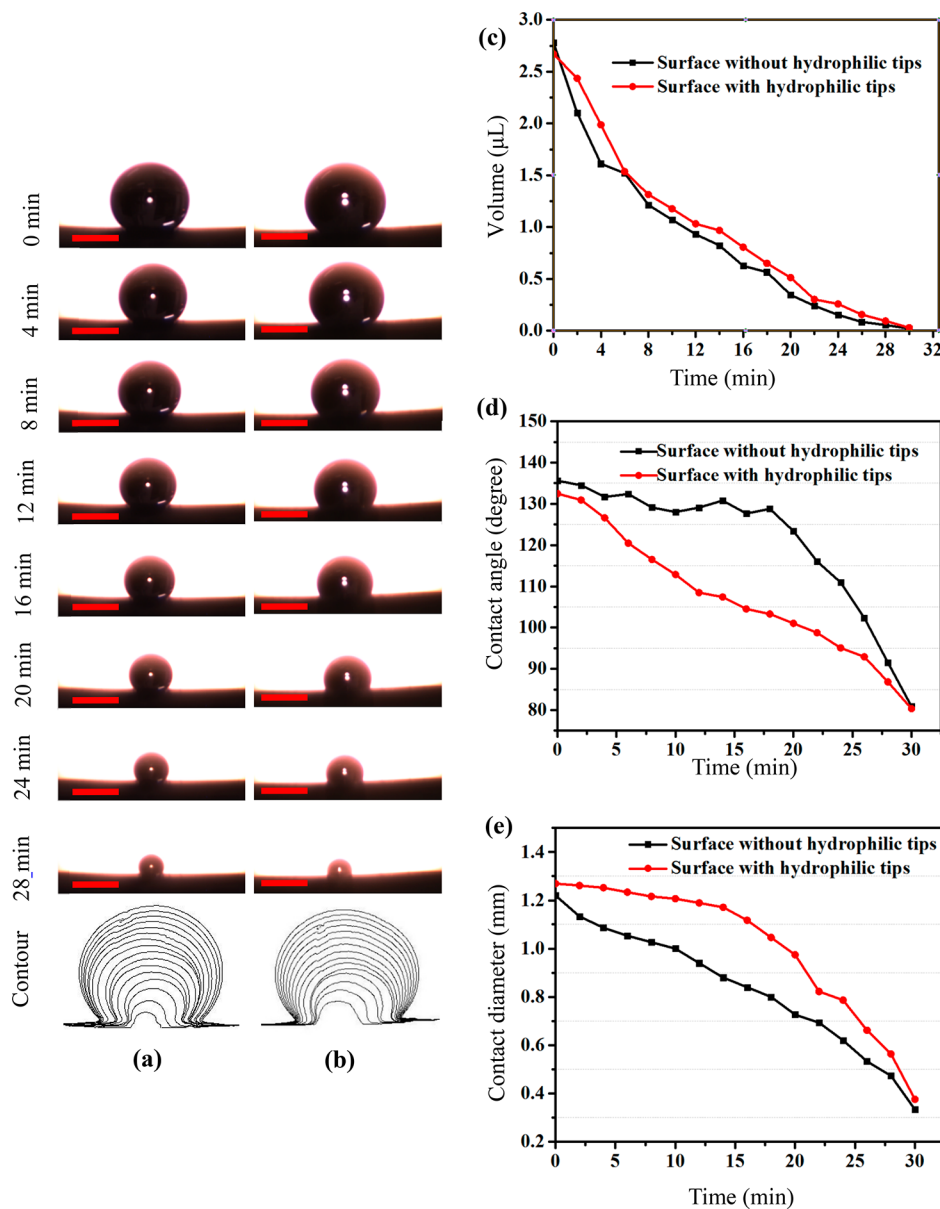| surface type	static angle (deg)	advancing angle (deg)	receding angle (deg)	contact angle hysteresis (deg)	sliding angle (deg)	depinning force (mN/m)
without hydrophilic tips	146 ± 2	147 ± 2	133 ± 2	14 ± 4	6 ± 1	10 ± 3
with hydrophilic tips	148 ± 2	154 ± 2	103 ± 2	51 ± 4	no sliding	45 ± 4

Figure 7. Water droplet evaporation test. (a, b) Images and contour of the droplets on the superhydrophobic surfaces without and with the decoration of hydrophilic tips, respectively. Scale bar in each image is 1 mm. (c) Change in droplet volumes during evaporation. (d) Change in droplet contact angles during evaporation. (e) Change in droplet contact diameters during evaporation.

the superhydrophobic surface with no decoration of hydrophilic tips were 147 ± 2° and 133 ± 2°, respectively, whereas those on the superhydrophobic surface decorated with hydrophilic tips were 154 ± 2° and 103 ± 2°, respectively. The result shows that the contact angle hysteresis (difference between the advancing and receding contact angles) is significantly increased by the hydrophilic tips, i.e., 51 ± 4° for the superhydrophobic surface decorated with hydrophilic tips vs 14 ± 4° for the superhydrophobic surface with no decoration of hydrophilic tips. As reported by Butt et al.,[53] the "microscopic" advancing contact angle of a droplet on poststructured surfaces

should be 180° irrespective of the structure dimensions, and the droplet pinning is solely determined by the receding boundary motion. The significant lowered receding contact angle on the superhydrophobic surface with hydrophilic tips mainly results in the high contact angle hysteresis and droplet retention. The significant difference in the droplet mobility and retention was also shown in the measurement of sliding angles (Figure 6e,f). The sliding angle, which was measured at the onset of the sliding motion, on the superhydrophobic surface with no decoration of hydrophilic tips was 6 ± 1° (Figure 6e). However, for the superhydrophobic surface decorated with

hydrophilic tips, the water droplet remained pinned on the surface even when the surface was inclined to 90°. Even when the surface was further tiled to be upside down, the droplet still clung to the surface with complete pinning (Figure 6f). This demonstrates that compared with the homogeneous hydrophobic tips, the hydrophilic nature of the metal tips contributes to the strong pinning effect on the droplet.

The depinning force per the unit length of the apparent droplet boundary (F_d), which quantifies the droplet retention, was also estimated according to the initial static contact angle (θ_e) and the receding contact angle (θ_r), expressed as[30]

$$F_d = \sigma(\cos\theta_r - \cos\theta_e)$$

where σ represents the liquid−gas interfacial tension (e.g., 72 mN/m at room conditions). The estimated depinning force of the droplet on the micropost superhydrophobic surface with hydrophilic tips (45 ± 4 mN/m) is 3 times greater than that (10 ± 3 mN/m) of the droplet on the superhydrophobic surface without hydrophilic tips. The result further shows that the hydrophilic tips significantly promote the droplet pinning and retention. The shape and size (the re-entrant shape and the increase of a solid fraction) of the fabricated tips can also modify the surface hydrophobicity and droplet retention, whereas the main effect of a re-entrant shape of the tip is to enhance the robustness of the suspended liquid−gas interface.[54,55] Regarding the increase of a solid fraction, however, its impact should be less significant than the effect of surface energy. The previous study suggested that the increase of a solid fraction only (i.e., with no change in the surface energy) should increase a droplet pinning force minutely; e.g., the increase of a solid fraction by 162.5% induced the increase of a depinning force no more than 87.5%.[54] However, in this study, the enhancement of a depinning force as high as 350% has been achieved by the increase in the solid fraction no more than 70%.

Droplet Evaporation. The effect of the hydrophilic tips of the superhydrophobic surfaces on the evaporative behaviors of the sessile water droplets was further investigated (see Movies 3 and 4). The hydrophobicity of the tips affects the pinning of a contact line of an evaporating droplet and hence the evolution and kinetics of the evaporating droplet.[56] Thus, the distinct behaviors of the droplet profile during the evaporation serve as another evidence of the different hydrophobicity achieved by the proposed fabrication method and their unique effects in the thermal transport phenomena. Figures 7a and 7b show the images and contours of an evaporating water droplet over time on the superhydrophobic surfaces without and with hydrophilic tips, respectively. The drop volume, contact angle, and contact diameter were measured from the captured images, as presented in Figures 7c, 7d, and 7e. There is no significant difference in the volume evolution of the droplet from the two different surfaces (Figure 7a). However, with regard to the evolution of droplet contact angles and contact diameters, the two surfaces demonstrate distinctive behaviors despite the almost same initial contact angles. The droplet contact angle on the surface without hydrophilic tips remained roughly constant (130°−135°) for the first ∼18 min (Figure 7d), while the contact diameter continuously decreased with time (Figure 7e). That corresponds to a constant contact angle (CCA) mode for an evaporating droplet, indicating that the droplet boundary depinned from the very beginning of evaporation. In contrast, the contact diameter of the droplet on the surface with hydrophilic tips remained roughly constant (1.2−1.3 mm) for

the first ∼14 min (Figure 7e), while the contact angle continuously decreased with time (Figure 7d). That corresponds to a constant contact diameter (CCD) mode, indicating that the droplet boundary was highly anchored on the hydrophilic tips. Based on the onset of the boundary detachment (the apparent decrease of the contact width), the apparent receding angles of droplets on the surfaces without and with hydrophilic tips estimated from Figure 7e are ∼135° and ∼107°, respectively, agreeing with the results measured by laterally dragging the droplets. The much smaller receding angle in the case with hydrophilic tips also indicates the greatly prolonged pinned boundary during the CCD mode. At the later evaporation stage, both droplets on the surfaces without and with hydrophilic tips translated to a mixed mode, where both the contact angle and the contact width decreased with time.

CONCLUSIONS

In this work, we have developed a heterogeneous super-hydrophobic surface decorated with hydrophilic tips, by exploiting a novel meniscus-confined electrodeposition method. Owning to the inherent Cassie−Baxter superhydrophobicity (i.e., capability of retaining air in cavities between hydrophobic microstructures) of the original superhydrophobic surface, the selective deposition of hydrophilic materials (nickel) only on the structural tips could be achieved. Such heterogeneous hydrophilic tips allow the superhydrophobic surface to have unique properties compared to conventionally (either slippery or sticky) superhydrophobic with homogeneous chemical coating, especially dynamic properties such as significantly enhanced droplet retention (i.e., higher contact angle hysteresis and depinning force) in the droplet movement, while the Cassie−Baxter wetting state is still sustained. The meniscus-confined electrodeposition method that we have developed is a convenient process that can be easily scaled up, since it is based on the electroplating technique that has been extensively used for surface coating and treatment for large-area substrates in manufacturing industries. The superhydrophobic surfaces with regulated droplet retention would be of great significance in many droplet-based applications such as biodetection,[57] inkjet printing,[58] evaporative cooling,[56] water harvesting,[59] and droplet transportation.[60] For example, a sticky superhydrophobic surface is desirable in the application of protein chips, where high contact angle (i.e., small footprint) as well as good adhesiveness of the droplet of analyte are both necessary to facilitate the detection.[57] Besides, the unique combination of hydrophilic pins on a superhydrophobic surface provides a promising approach of realizing long-term gas retaining for underwater applications, such as drag reduction in turbulent flow,[33] anticorrosion,[10] and antifouling surfaces.[9]

ASSOCIATED CONTENT

Ⓢ Supporting Information

The Supporting Information is available free of charge on the ACS Publications website at DOI: 10.1021/acs.langmuir.7b03014.

> Initiation of electrodeposition around the sharp edges of microposts' top surfaces; scanning electron microscope (SEM) image (inclined views) of the microposts; measurement of contact angles of the electrolyte droplet on the surfaces; scanning electron microscope (SEM) image (side view) of the electrodeposition result due to

the failure of Cassie−Baxter wetting state; table of the DRIE parameters (PDF)

Movies 1−4: videos of the underwater immersion test and of the droplet evaporation test (ZIP)

■ AUTHOR INFORMATION

Corresponding Author

*E-mail: guangyi@nankai.edu.cn (G.S.).

ORCID 🟢

Chang-Hwan Choi: 0000-0003-2715-7393

Guangyi Sun: 0000-0003-1362-750X

Notes

The authors declare no competing financial interest.

■ REFERENCES

(1) Callies, M.; Quéré, D. On Water Repellency. *Soft Matter* **2005**, *1*, 55−61.

(2) Cassie, A. B. D.; Baxter, S. Wettability of Porous Surfaces. *Trans. Faraday Soc.* **1944**, *40*, 546−551.

(3) Wenzel, R. N. Resistance of Solid Surfaces to Wetting by Water. *Ind. Eng. Chem.* **1936**, *28*, 988−994.

(4) Qu, X.; Boreyko, J. B.; Liu, F.; Agapov, R. L.; Lavrik, N. V.; Retterer, S. T.; Feng, J. J.; Collier, C. P.; Chen, C. H. Self-propelled Sweeping Removal of Dropwise Condensate. *Appl. Phys. Lett.* **2015**, *106*, 221601.

(5) Neinhuis, C.; Barthlott, W. Characterization and Distribution of Water-repellent, Self-cleaning Plant Surfaces. *Ann. Bot. (Oxford, U. K.)* **1997**, *79*, 667−677.

(6) Fürstner, R.; Barthlott, W.; Neinhuis, C.; Walzel, P. Wetting and Self-cleaning Properties of Artificial Superhydrophobic Surfaces. *Langmuir* **2005**, *21*, 956−961.

(7) Nishimoto, S.; Bhushan, B. Bioinspired Self-cleaning Surfaces with Superhydrophobicity, Superoleophobicity, and Superhydrophilicity. *RSC Adv.* **2013**, *3*, 671−690.

(8) Hizal, F.; Rungraeng, N.; Lee, J.; Jun, S.; Busscher, H. J.; van der Mei, H. C.; Choi, C. H. Nanoengineered Superhydrophobic Surfaces of Aluminum with Extremely Low Bacterial Adhesivity. *ACS Appl. Mater. Interfaces* **2017**, *9*, 12118−12129.

(9) Tesler, A. B.; Kim, P.; Kolle, S.; Howell, C.; Ahanotu, O.; Aizenberg, J. Extremely Durable Biofouling-resistant Metallic Surfaces Based on Electrodeposited Nanoporous Tungstite Films on Steel. *Nat. Commun.* **2015**, *6*, 8649.

(10) Su, F.; Yao, K. Facile Fabrication of Superhydrophobic Surface with Excellent Mechanical Abrasion and Corrosion Resistance on Copper Substrate by a Novel Method. *ACS Appl. Mater. Interfaces* **2014**, *6*, 8762−8770.

(11) Ishizaki, T.; Hieda, J.; Saito, N.; Saito, N.; Takai, O. Corrosion Resistance and Chemical Stability of Super-hydrophobic Film Deposited on Magnesium Alloy AZ31 by Microwave Plasma-enhanced Chemical Vapor Deposition. *Electrochim. Electrochim. Acta* **2010**, *55*, 7094−7101.

(12) Jeong, C.; Lee, J.; Sheppard, K.; Choi, C. H. Air-impregnated Nanoporous Anodic Aluminum Oxide Layers for Enhancing the Corrosion Resistance of Aluminum. *Langmuir* **2015**, *31*, 11040−11050.

(13) Sarshar, M. A.; Swarctz, C.; Hunter, S.; Simpson, J.; Choi, C. H. Effects of Contact Angle Hysteresis on Ice Adhesion and Growth on Superhydrophobic Surfaces under Dynamic Flow Conditions. *Colloid Polym. Sci.* **2013**, *291*, 427−435.

(14) Jung, S.; Dorrestijn, M.; Raps, D.; Das, A.; Megaridis, C. M.; Poulikakos, D. Are Superhydrophobic Surfaces Best for Icephobicity? *Langmuir* **2011**, *27*, 3059−3066.

(15) Mishchenko, L.; Hatton, B.; Bahadur, V.; Taylor, J. A.; Krupenkin, T.; Aizenberg, J. Design of Ice-free Nanostructured Surfaces Based on Repulsion of Impacting Water Droplets. *ACS Nano* **2010**, *4*, 7699−7707.

(16) Emelyanenko, A. M.; Boinovich, L. B.; Bezdomnikov, A. A.; Chulkova, E. V.; Emelyanenko, K. A. Reinforced Superhydrophobic Coating on Silicone Rubber for Longstanding Anti-icing Performance in Severe Conditions. *ACS Appl. Mater. Interfaces* **2017**, *9*, 24210−24219.

(17) Miljkovic, N.; Wang, E. N. Condensation Heat Transfer on Superhydrophobic Surfaces. *MRS Bull.* **2013**, *38*, 397−406.

(18) Paven, M.; Papadopoulos, P.; Schöttler, S.; Deng, X.; Mailänder, V.; Vollmer, D.; Butt, H. J. Super Liquid-repellent Gas Membranes for Carbon Dioxide Capture and Heart−lung Machines. *Nat. Commun.* **2013**, *4*, 2512.

(19) Liu, J.; Guo, H.; Zhang, B.; Qiao, S.; Shao, M.; Zhang, X.; Wang, J.; et al. Guided Self-Propelled Leaping of Droplets on a Micro-Anisotropic Superhydrophobic Surface. *Angew. Chem.* **2016**, *128*, 4337−4341.

(20) Xue, X.; Yu, C.; Wang, J.; Jiang, L. Superhydrophobic Cones for Continuous Collection and Directional Transportation of CO_2 Microbubbles in CO_2 Supersaturated Solutions. *ACS Nano* **2016**, *10*, 10887−10893.

(21) Ko, D. H.; Ren, W.; Kim, J. O.; Wang, J.; Wang, H.; Sharma, S.; Faustini, M.; Kim, D. P. Superamphiphobic Silicon-nanowire-embedded Microsystem and in-contact Flow Performance of Gas and Liquid Streams. *ACS Nano* **2016**, *10*, 1156−1162.

(22) Lee, C.; Choi, C. H.; Kim, C. J. Superhydrophobic Drag Reduction in Laminar Flows: A Critical Review. *Exp. Fluids* **2016**, *57*, 176.

(23) Aljallis, E.; Sarshar, M. A.; Datla, R.; Sikka, V.; Jones, A.; Choi, C. H. Experimental Study of Skin Friction Drag Reduction on Superhydrophobic Flat Plates in High Reynolds Number Boundary Layer Flow. *Phys. Fluids* **2013**, *25*, 025103.

(24) Park, H.; Sun, G.; Kim, C. J. Superhydrophobic Turbulent Drag Reduction as A Function of Surface Grating Parameters. *J. Fluid Mech.* **2014**, *747*, 722−734.

(25) Xu, M.; Sun, G.; Kim, C. J. Infinite Lifetime of Underwater Superhydrophobic States. *Phys. Rev. Lett.* **2014**, *113*, 136103.

(26) Cho, K. H.; Chen, L. J. Fabrication of Sticky and Slippery Superhydrophobic Surfaces Via Spin-coating Silica Nanoparticles onto Flat/patterned Substrates. *Nanotechnology* **2011**, *22*, 445706.

(27) Bhushan, B.; Her, E. K. Fabrication of Superhydrophobic Surfaces with High and Low Adhesion Inspired from Rose Petal. *Langmuir* **2010**, *26*, 8207−8217.

(28) Boscher, N. D.; Duday, D.; Verdier, S.; Choquet, P. Single-step Process for the Deposition of High Water Contact Angle and High Water Sliding Angle Surfaces by Atmospheric Pressure Dielectric Barrier Discharge. *ACS Appl. Mater. Interfaces* **2013**, *5*, 1053−1060.

(29) Jeong, C.; Choi, C. H. Single-step Direct Fabrication of Pillar-on-pore Hybrid Nanostructures in Anodizing Aluminum for Superior Superhydrophobic Efficiency. *ACS Appl. Mater. Interfaces* **2012**, *4*, 842−848.

(30) Xu, W.; Choi, C. H. From Sticky to Slippery Droplets: Dynamics of Contact Line Depinning on Superhydrophobic Surfaces. *Phys. Rev. Lett.* **2012**, *109*, 024504.

(31) Nosonovsky, M.; Bhushan, B. Lotus Versus Rose: Biomimetic Surface Effects. In *Green Tribology*; Nosonovsky, M., Bhushan, B., Eds.; Springer: Berlin, 2012; Chapter 2, pp 25−40.

(32) Yeh, K. Y.; Cho, K. H.; Yeh, Y. H.; Promraksa, A.; Huang, C. H.; Hsu, C. C.; Chen, L. J. Observation of The Rose Petal Effect over Single-and Dual-scale Roughness Surfaces. *Nanotechnology* **2014**, *25*, 345303.

(33) Barthlott, W.; Schimmel, T.; Wiersch, S.; Koch, K.; Brede, M.; Barczewski, M.; Walheim, S.; Weis, A.; Kaltenmaier, A.; Leder, A.; Bohn, H. F. The Salvinia Paradox: Superhydrophobic Surfaces with

Hydrophilic Pins for Air Retention under Water. *Adv. Mater.* **2010**, *22*, 2325−2328.

(34) Hejazi, V.; Nosonovsky, M. Contact Angle Hysteresis in Multiphase Systems. *Colloid Polym. Sci.* **2013**, *291*, 329−338.

(35) Chang, F. M.; Hong, S. J.; Sheng, Y. J.; Tsao, H. K. High Contact Angle Hysteresis of Superhydrophobic Surfaces: Hydrophobic Defects. *Appl. Phys. Lett.* **2009**, *95*, 064102.

(36) Yuan, Y.; Lee, T. R. Contact Angle and Wetting Properties. In *Surface Science Techniques*; Bracco, G., Holst, B., Eds.; Springer: Berlin, 2013; Chapter 2, pp 3−34.

(37) Liu, Y.; Choi, C. H. Condensation-induced Wetting State and Contact Angle Hysteresis on Superhydrophobic Lotus Leaves. *Colloid Polym. Sci.* **2013**, *291*, 437−445.

(38) Lee, C.; Kim, C. J. Underwater Restoration and Retention of Gases on Superhydrophobic Surfaces for Drag Reduction. *Phys. Rev. Lett.* **2011**, *106*, 014502.

(39) Cui, Y.; Paxson, A. T.; Smyth, K. M.; Varanasi, K. K. Hierarchical Polymeric Textures via Solvent-induced Phase Transformation: a Single-step Production of Large-area Superhydrophobic Surfaces. *Colloids Surf., A* **2012**, *394*, 8−13.

(40) Sarshar, M. A.; Xu, W.; Choi, C. H. Correlation between Contact Line Pinning and Contact Angle Hysteresis on Heterogeneous Surfaces: A Review and Discussion. *Adv. Contact Angle, Wettability Adhes.* **2013**, *001*, 1−18.

(41) Tricinci, O.; Terencio, T.; Mazzolai, B.; Pugno, N. M.; Greco, F.; Mattoli, V. 3D Micropatterned Surface Inspired by Salvinia Molesta via Direct Laser Lithography. *ACS Appl. Mater. Interfaces* **2015**, *7*, 25560−25567.

(42) Vishwakarma, N. K.; Singh, A. K.; Hwang, Y. H.; Ko, D. H.; Kim, J. O.; Babu, A. G.; Kim, D. P. Integrated CO_2 Capture-fixation Chemistry via Interfacial Ionic Liquid Catalyst in Laminar Gas/liquid Flow. *Nat. Commun.* **2017**, *8*, 14676.

(43) Babu, D. J.; Mail, M.; Barthlott, W.; Schneider, J. J. Superhydrophobic Vertically Aligned Carbon Nanotubes for Biomimetic Air Retention under Water (Salvinia Effect). *Adv. Mater. Interfaces* **2017**, *4*, 1700273.

(44) Hu, J.; Yu, M. F. Meniscus-confined Three-dimensional Electrodeposition for Direct Writing of Wire Bonds. *Science* **2010**, *329*, 313−316.

(45) Suryavanshi, A. P.; Hu, J.; Yu, M. F. Meniscus-Controlled Continuous Fabrication of Arrays and Rolls of Extremely Long Micro- and Nano-Fibers. *Adv. Mater.* **2008**, *20*, 793−796.

(46) Kim, J. T.; Seol, S. K.; Pyo, J.; Lee, J. S.; Je, J. H.; Margaritondo, G. Three-Dimensional Writing of Conducting Polymer Nanowire Arrays by Meniscus-Guided Polymerization. *Adv. Mater.* **2011**, *23*, 1968−1970.

(47) Resnick, P. R.; Buck, W. H. Teflon® AF: A Family of Amorphous Fluoropolymers with Extraordinary Properties. In *Fluoropolymers 2*; Hougham, G., Cassidy, P. E., Johns, K., Davidson, T., Eds.; Springer: New York, 2002; Chapter 2, pp 25−33.

(48) Pilat, D. W.; Papadopoulos, P.; Schaffel, D.; Vollmer, D.; Berger, R.; Butt, H. J. Dynamic Measurement of the Force Required to Move a Liquid Drop on A Solid Surface. *Langmuir* **2012**, *28*, 16812−16820.

(49) Lou, H. H.; Huang, Y. L. Electroplating. In *Encyclopedia of Chemical Processing*; Lee, S., Ed.; CRC Press: 2005; Vol. 2, pp 839−849.

(50) Govardhan, R. N.; Srinivas, G. S.; Asthana, A.; Bobji, M. S. Time Dependence of Effective Slip on Textured Hydrophobic Surfaces. *Phys. Fluids* **2009**, *21*, 052001.

(51) Larmour, I. A.; Bell, S. E.; Saunders, G. C. Remarkably Simple Fabrication of Superhydrophobic Surfaces using Electroless Galvanic Deposition. *Angew. Chem., Int. Ed.* **2007**, *46*, 1710−1712.

(52) Zuhlke, C. A.; Anderson, T. P.; Li, P.; Lucis, M. J.; Roth, N.; Shield, J. E.; Terry, B.; Alexander, D. R. Superhydrophobic Metallic Surfaces Functionalized via Femtosecond Laser Surface Processing for Long Term Air Film Retention When Submerged in Liquid. *Proc. SPIE* **2015**, *9351*, 93510J−1.

(53) Schellenberger, F.; Encinas, N.; Vollmer, D.; Butt, H. J. How Water Advances on Superhydrophobic Surfaces. *Phys. Rev. Lett.* **2016**, *116*, 096101.

(54) Dufour, R.; Harnois, M.; Thomy, V.; Boukherroub, R.; Senez, V. Contact Angle Hysteresis Origins: Investigation on Super-omniphobic Surfaces. *Soft Matter* **2011**, *7*, 9380−9387.

(55) Liu, T.; Kim, C. J. Turning a Surface Superrepellent Even to Completely Wetting Liquids. *Science* **2014**, *346*, 1096−1100.

(56) Shanahan, M. E. R.; Sefiane, K.; Moffat, J. R. Dependence of Volatile Droplet Lifetime on the Hydrophobicity of the Substrate. *Langmuir* **2011**, *27*, 4572−4577.

(57) Tsougeni, K.; Tserepi, A.; Constantoudis, V.; Gogolides, E.; Petrou, P. S.; Kakabakos, S. E. Plasma Nanotextured PMMA Surfaces for Protein Arrays: Increased Protein Binding and Enhanced Detection Sensitivity. *Langmuir* **2010**, *26*, 13883−13891.

(58) Erbil, H. Y. Evaporation of Pure Liquid Sessile and Spherical Suspended Drops: A Review. *Adv. Colloid Interface Sci.* **2012**, *170*, 67−86.

(59) Parker, A. R.; Lawrence, C. R. Water Capture by A Desert Beetle. *Nature* **2001**, *414*, 33−34.

(60) Xu, W.; Palumbo, A.; Xu, J.; Jiang, Y.; Choi, C. H.; Yang, E. H. On-Demand Capture and Release of Organic Droplets using Surfactant-Doped Polypyrrole Surfaces. *ACS Appl. Mater. Interfaces* **2017**, *9*, 23119−23127.